Acta Crystallographica Section B
Structural Science
ISSN 0108-7681

Structural phase transitions in tetra(isopropylammonium) decachlorotricadmate(II), $[(CH_3)_2CHNH_3]_4Cd_3Cl_{10}$, crystal with a two-dimensional cadmium(II) halide network

Anna Gagor,[a]* Alicja Waśkowska,[a] Zbigniew Czapla[b,c] and Slawomir Dacko[c]

[a]Institute of Low Temperature and Structure Research, Polish Academy of Sciences, Okólna 2, 50-422 Wrocław, Poland, [b]Department of Physics, Opole University of Technology, Ozimska 75, 45-271 Opole, Poland, and [c]Institute of Experimental Physics, University of Wrocław, M Borna 9, 50-204 Wrocław, Poland

Correspondence e-mail: a.gagor@int.pan.wroc.pl

Received 6 September 2010
Accepted 28 December 2010

Single crystals of tetra(isopropylammonium) decachlorotricadmate(II) as a rare example of a two-dimensional cadmium(II) halide network of $[Cd_3Cl_{10}]_n^{4-}$ have been synthesized and characterized by means of calorimetry and X-ray diffraction. The crystals exhibit polymorphism in a relatively narrow temperature range (three phase transitions at 353, 294 and 259 K). Our main focus was to establish the mechanism of these successive transformations. The crystal structure was solved and refined in the space group *Cmce* at 375 K (Phase I), *Pbca* at 320 K (Phase II) and $P2_12_12_1$ (Phase III) at 275 K in the same unit-cell metric. The structure is composed of face-sharing polyanionic $[Cd_3Cl_{10}]^{4-}$ units which are interconnected at the bridging Cl atom into four-membered rings forming a unique two-dimensional network of $[Cd_3Cl_{10}]_n^{4-}$. The interstitial voids within the network are large enough to accommodate isopropylammonium cations and permit thermally activated rotations. While in Phase I isopropylammonium tetrahedra rotate almost freely about the C—N bond, the low-temperature phases are the playground of competition between the thermally activated disorder of isopropylammonium cations and stabilizing N—H···Cl hydrogen-bond interactions. The transition from Phase I to II is dominated by a displacive mechanism that leads to significant rearrangement of the polyanionic units. Cation order–disorder phenomena become prominent at lower temperatures.

1. Introduction

Unusual structural architectures are formed in halogenocadmate(II) compounds. Owing to the chemical flexibility (the flexibility which accommodates different organic counterions as well as inorganic components) of these hybrid organic–inorganic materials, it is possible to create different crystal structures to optimize their physical properties (Costin-Hogan *et al.*, 2008; Thorn *et al.*, 2005). Cadmium compounds are also interesting from the point of view of the role of this metal in biological processes (Marzili *et al.*, 1980).

Depending on the size of organic counterions and the strength of hydrogen-bond interactions between the polar protonated amine groups of organic cations and halogen atoms, various anionic substructures may be generated: such as isolated octahedral and tetrahedral units, one-dimensional linear chains, ribbon-like structures and two-dimensional layers, by sharing triangular faces, edges or vertices of octahedra.

A wide variety of stoichiometries have been found in this class of material, *e.g.* $[CdCl_3]$ (Peral *et al.*, 2000), $[Cd_3Cl_9]$ (Jian *et al.*, 2006), $[CdCl_4]$, $[Cd_3Cl_{10}]$ (Chaabane *et al.*, 2008), $[CdCl_6]$ (Sakida *et al.*, 2003) and $[Cd_3Cl_{11}]$ (Waśkowska *et al.*, 1990).

Table 1
The transition temperatures, enthalpies and entropies for $[(CH_3)_2CHNH_3]_4Cd_3Cl_{10}$ crystal obtained on cooling.

T_{tr} (K)	Character of PT	ΔH (J mol^{-1})	ΔS (J mol^{-}K^{-})
353	First order	11 (3) × 10^2	3 (1)
294	Second order	–	–
259	First order	27 (8) × 10^2	9 (3)

$[C_6H_{10}N_2]_2Cd_3Cl_{10}$ and $[C_4H_{14}N_2]Cd_3Cl_{10}$ possess an interesting structure where the anionic substructure is built of one-dimensional polymeric $(Cd_3Cl_{10})_n^{4n-}$ chains (Bonamartini-Corradi *et al.*, 1993). $[C_6H_8N]_4^+[Cd_3Cl_{10}]^{4-}$, on the other hand, crystallizes with a two-dimensional layered network of $(Cd_3Cl_{10})^{4-}$ linear trimers that are interconnected by bridging corner-shared chlorides (Costin-Hogan *et al.*, 2008).

Some organic–inorganic compounds containing cadmium adopt different polymorphic forms and exhibit complex structural phase transitions that are associated with freezing and reorientation of the cations and deformation of the anionic substructure. Tetramethylammonium trichlorocadmate $(CH_3)_4NCdCl_3$ exhibits two successive structure transformations, and the low-temperature phases show ferroelastic twinning (Peral *et al.*, 2000; Mulla-Osman *et al.*, 2000). Successive phase transitions were also found in $[(CH_3)_2NH_2]_5Cd_3Cl_{11}$ (Czapla *et al.*, 1989), for which X-ray diffraction as well as optical studies (Czapla *et al.*, 1994) showed the incommensurate character of the intermediate phase. Phase transformations were also observed in isopropylammonium trichlorocadmate, $[(CH_3)_2CHNH_3]CdCl_3$ (Krzewska *et al.*, 1992).

In searching for new original anionic architectures in halogenocadmate systems exhibiting structural phase transitions we obtained the new crystalline organic–inorganic substance $[(CH_3)_2CHNH_3]_4Cd_3Cl_{10}$ containing isopropylammonium cations and chlorocadmate anions. This paper presents the thermal properties of the compound and the crystal structures of three polymorphic phases along with a discussion of the structural mechanisms of the phase transitions.

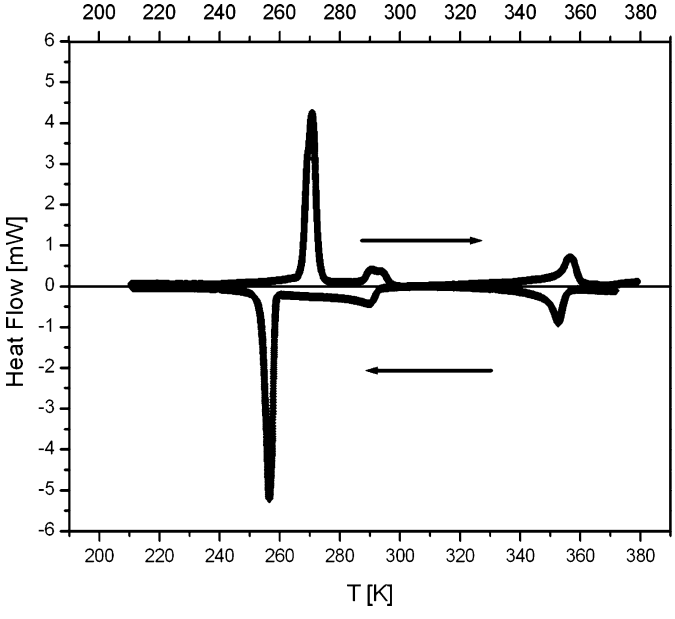

Figure 1
The observed temperature dependence of heat flow for the $[(CH_3)_2CHNH_3]_4Cd_3Cl_{10}$ crystal.

2. Synthesis and crystal growth

Colorless crystals were obtained from aqueous solution containing isopropylammonium chloride and cadmium chloride in a 3:1 molar ratio by slow evaporation at a constant temperature of 303 K. The formula of the product is $[(CH_3)_2CHNH_3]_4Cd_3Cl_{10}$ (or $C_{12}H_{40}N_4Cl_{10}Cd_3$).

Element	C	H	N	Cl	Cd
%Theor.	15.46	4.33	6.0	38	36.2
%Exp.	15.5 (2)	4.2 (5)	5.9 (2)	37 (1)	37 (1)

The crystals were easily grown and they exhibited a distinct cleavage plane perpendicular to the *b* axis. As-grown crystals were dissolved in water and the solution was evaporated. In the first stage this treatment gave crystals of $[(CH_3)_2CHNH_3]CdCl_3$. This indicates that $[(CH_3)_2CHNH_3]_4Cd_3Cl_{10}$ crystals do not grow from stoichiometric quantities of the components.

3. Thermal analysis

Differential scanning calorimetry (DSC) measurements were carried out using a Perkin–Elmer TMA-7 calorimeter with rates ranging from 10 to 20 K min^{-1}. The typical dependence of heat flow connected with phase transitions after subtraction of the baseline is presented in Fig. 1.

DSC studies revealed a sequence of phase transitions at 353, 294 and 259 K on cooling. The transition at 353 K is first order with a small temperature hysteresis, but it resembles (is close to) second order. Despite the fact that the phase transition at 294 K on heating resembles first order, we classify it as continuous on the basis of the shape of the thermal anomaly on cooling. Preliminary heat-capacity measurements unambiguously point to the second-order character of this transformation (J. Przesławski, private communication). The transition at 260 K is typically first order with a noticeable temperature hysteresis.

The temperatures and average enthalpies, and corresponding entropies of the observed sequence of phase transitions are presented in Table 1.

DSC data obtained for different samples and different heating/cooling rates show a wide range of enthalpy and entropy values. Therefore, DSC data have considerable uncertainty (*ca* 30%) and we treat them as more indicative than quantitative.

Table 2
Experimental details.

For all structures: $C_{12}H_{40}Cd_3Cl_{10}N_4$, M_r = 932.18, Z = 4. Experiments were carried out with Mo $K\alpha$ radiation. Absorption was corrected for by multi-scan methods, *CrysAlis RED*, Oxford Diffraction Ltd, Version 1.171.32.6 (release 21-05-2007 CrysAlis171 .NET, compiled May 21 2007, 16:32:00). Empirical absorption correction using spherical harmonics, implemented in *SCALE3 ABSPACK* scaling algorithm.

	Cmce	*Pbca*	$P2_12_12_1$
Crystal data			
Crystal system, space group	Orthorhombic, *Cmce*	Orthorhombic, *Pbca*	Orthorhombic, $P2_12_12_1$
Phase, temperature (K)	I, 375	II, 320	III, 275
a, b, c (Å)	7.4634 (2), 22.0476 (10), 19.6139 (9)	7.4298 (5), 22.0790 (5), 19.4442 (6)	7.3918 (2), 22.0135 (7), 19.3938 (5)
V (Å^3)	3227.5 (2)	3189.7 (2)	3155.75 (15)
μ (mm^{-1})	2.79	2.83	2.86
Crystal size (mm)	0.25 × 0.2 × 0.08	0.25 × 0.2 × 0.08	0.25 × 0.2 × 0.08
Data collection			
Diffractometer	KUMA KM4-CCD	KUMA KM4-CCD	KUMA KM4-CCD
T_{min}, T_{max}	0.49, 0.79	0.49, 0.79	0.49, 0.79
No. of measured, independent and observed [$I > 2\sigma(I)$] reflections	14 304, 2333, 1659	26 736, 3010, 2449	25 404, 5945, 4686
R_{int}	0.031	0.030	0.043
Refinement			
$R[F^2 > 2\sigma(F^2)]$, $wR(F^2)$, S	0.025, 0.054, 0.90	0.024, 0.062, 1.01	0.028, 0.047, 0.83
No. of reflections	2333	3010	5945
No. of parameters	101	146	267
No. of restraints	0	6	6
$\Delta\rho_{max}$, $\Delta\rho_{min}$ (e Å^{-3})	0.35, −0.41	0.36, −0.49	0.52, −0.37
Absolute structure	–	–	Flack (1983)
Flack parameter	–	–	0.45 (4)

4. Crystal structure

4.1. X-ray data collection and processing

X-ray diffraction intensity data were collected on a KUMA KM4-CCD diffractometer operating in κ geometry and equipped with a two-dimensional CCD detector. Graphite-monochromated Mo $K\alpha$ radiation was used. Data were collected in ω-scan mode with $\Delta\omega = 1.0^\circ$ using the *CrysAlis CCD* program (Oxford Diffraction, 2005). Diffraction data were collected at 375, 325, 275 and 260 K. The sample was first heated to the prototype Phase I (375 K) and then the data for individual phases were collected on cooling. An open-flow nitrogen cryosystem (Oxford Cryosystem, covering the temperature range 90–320 K) was used for experiments from 295 to 235 K, while a simple high-temperature attachment with a hot-air flow (Kuma Diffraction, covering the temperature range 300–770 K) was used for the experiments at temperatures ranging between 295 and 385 K. *CrysAlis RED* software (Oxford Diffraction, 2008) was used for data processing. An empirical absorption correction was applied using the spherical harmonics implemented in the *SCALE3 ABSPACK* scaling algorithm. The structure was solved by direct methods and refined by the full-matrix least-squares method using *SHELX*97 (Sheldrick, 2008). In all phases the H atoms were located from geometry and constrained in their positions as 'riding groups' with N—H and C—H distances restrained to 0.89 and 0.96 Å, and with U_{iso}(H) = 1.2 and 1.5 × U_{eq} of the corresponding parent atom. In all phases, however, only those H atoms that were bonded to non-disordered C

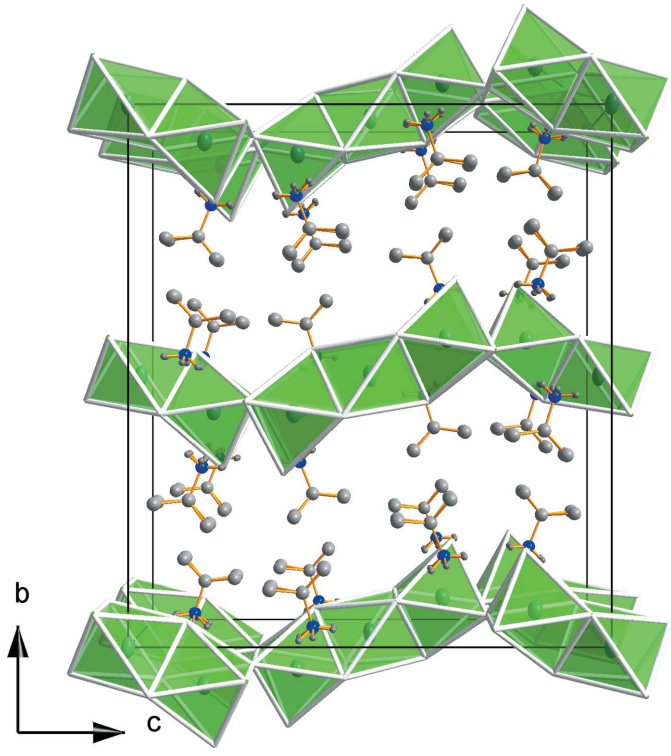

Figure 2
The projection of the $[(CH_3)_2CHNH_3]_4Cd_3Cl_{10}$ structure at 375 K in Phase 1 along [100]. The cations are disordered over the (100) plane. H atoms bonded to disordered atoms are omitted for clarity.

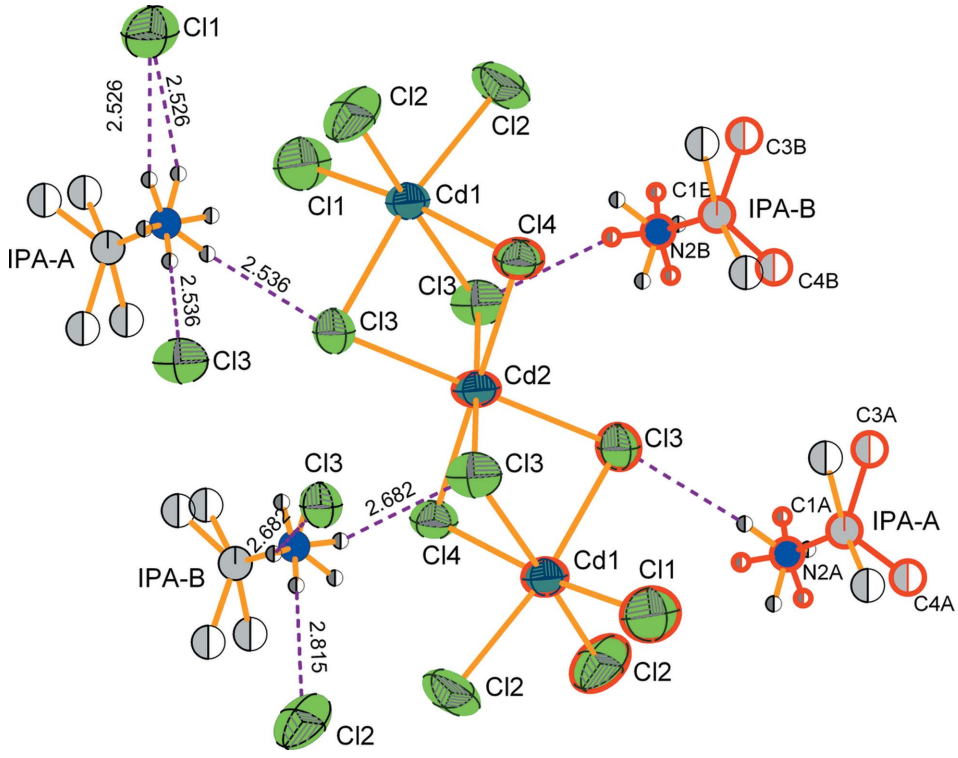

Figure 3
Elemental anionic motif $[Cd_3Cl_{10}]^{4-}$ building an anionic substructure along with disordered isopropylammonium cations at T = 375 K. The dashed lines represent hydrogen bonds. All possible N—H···Cl contacts for IPA-*A* and IPA-*B* are marked with the appropriate H···Cl distances. The red bordered atoms represent symmetrically nonequivalent positions forming an asymmetric unit in the prototype Phase I; half-colored atoms possess 0.5 occupancy. H atoms bonded to disordered atoms are omitted for clarity. This figure is in color in the electronic version of this paper.

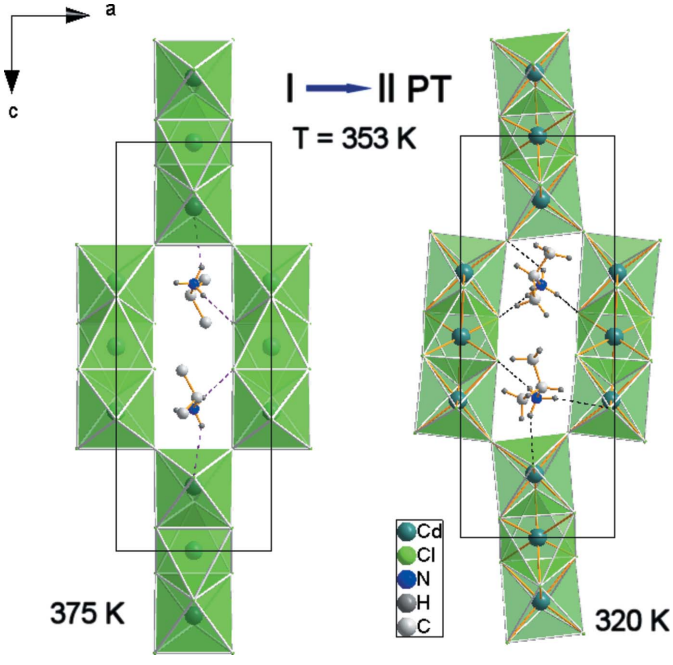

Figure 4
Transformation of the anionic substructure in the phase transition from Phase I to Phase II at 353 K. H atoms bonded to disordered atoms are omitted for clarity.

atoms were included in the refinement. The valence of cadmium has been calculated from the refined structure models using the bond-valence method (Brown, 1996). More details on data collection and reduction are given in Table 2.

$[(CH_3)_2CHNH_3]_4Cd_3Cl_{10}$ exhibits several temperature-dependent phase transitions and therefore the structures of the individual phases were studied. The structure of the high-temperature prototypic Phase I was solved in the space group *Cmce* (No. 64), suggested by averaging the reflection intensities and systematic absences. On cooling to 355 K the symmetry changes to *Pbca* (No. 61) Phase II, then at 294 K the structure transforms to Phase III with $P2_12_12_1$ symmetry (No. 19), and finally below 260 K to monoclinic Phase IV with $P12_1/a1$ symmetry. The crystal structure was solved and refined for the first three phases. Owing to the twinning and cracking accompanying the crystal system change from orthorhombic to monoclinic at the first-order phase transition III to IV, the structure of Phase IV was not solved. Averaging of the main twin component (that indexed 55% of the measured peaks) as well as careful analysis of reciprocal-space reconstructions and systematic absences led to only one possible space group ($P2_1/a$ at 235 K). Difference-Fourier maps allowed localization of the anionic substructure, although refinement based on the intensity data prepared in *CrysAlisPro* (software which provides the tools for simultaneous indexing of different twin components) resulted in a poor fit (R factor $\simeq 0.27$). The phase transition from *Cmce* to *Pbca* is of klassengleich type; the crystal class does not change (*mmm* → *mmm*). The remaining transitions (from *Pbca* to $P2_12_12_1$ and then to $P2_1/a$) are *translationengleiche*; crystal class changes (from *mmm* to 222 and finally to 2/*m*). Unit-cell periodicity is preserved during the transformations. The structures of the individual phases are presented in Figs. 2–5.

4.2. Phase I

At high temperature the parent Phase I $[(CH_3)_2CHNH_3]_4Cd_3Cl_{10}$ (abbreviated as IPACdCl) adopts the orthorhombic space group *Cmce*. The asymmetric unit contains two independent isopropylammonium cations (denoted as IPA-*A* and IPA-*B*), and two Cd and four Cl atoms. Cd atoms are located in two (2/*m*.. and *m*..) sites with octa-

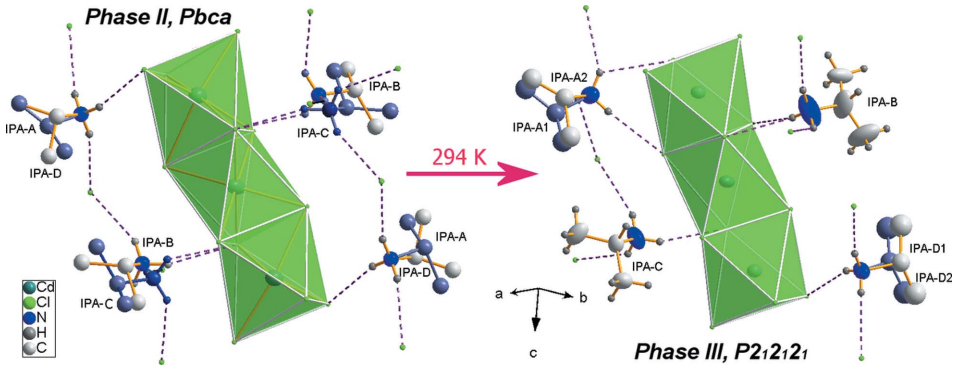

Figure 5
Change in the positional disorder of isopropylammonium cations observed after transformation from Phase II (*Pbca*) to Phase III ($P2_12_12_1$) at 294 K. Possible H···Cl contacts are marked as dashed lines. The occupancy of the disordered positions in both phases for IPA-*A* and IPA-*D* is 0.5, whereas the occupancy of disordered IPA-*B* and IPA-*C* in Phase II is 0.45 (1) and 0.55 (1). H atoms bonded to disordered atoms are omitted for clarity.

hedral coordination by Cl atoms. Face-sharing $CdCl_6$ octahedra form a $[Cd_3Cl_{10}]^{4-}$ polyanion that is an elementary block in building the anionic substructure. The $CdCl_6$ octahedra are distorted. In the *m*.. symmetry octahedron the Cd1—Cl_6 distances range from 2.4839 (5) to 2.7126 (3) Å, whereas the octahedron of 2/*m*.. symmetry is compressed as the two axial Cd2—Cl4 bonds are shorter by 0.066 Å than those in the equatorial plane. The mean Cd—Cl_6 distances [2.6443 (3) and 2.6343 (3) Å] are comparable, however, to those observed in similar cadmium halide anions (Noiret *et al.*, 2004; Morosin, 1972; Lamhamdi *et al.*, 2009). Selected distances are summarized in Table 3.

The $(Cd_3Cl_{10})^{4-}$ anions form four-membered rings interconnected by corners at the bridging Cl atom in a two-dimensional network of $(Cd_3Cl_{10})_n^{4-}$ nearly perpendicular to the *b* axis. These corner-sharing linear trimers $(Cd_3Cl_{10})^{4-}$ give a rare example of a two-dimensional cadmium(II) halide network that has only been reported for tetraanilinium decachlorocadmium (Costin-Hogan *et al.*, 2008) and its bromocadmium analog (Ishihara *et al.*, 1994).

The large interstitial voids within the network are occupied by the IPA counterions, which are disordered. Fig. 2 shows the crystal structure packing as seen in the [100] direction, whereas Fig. 3 presents the anionic motif and structure of the disordered cations. The disorder of the IPA groups drives from the fact that the *m*.. site point-group symmetry is higher than the real symmetry of cations. Thus, cations are disordered over two different positions about the mirror plane through the C1*A*—N2*A* and C1*B*—N2*B* bonds. Conversion between two statisticaly occupied positions must be realised by rotation of the whole cation along the C—N bond. Both IPA cations with amine groups are directed towards the polyanionic layer and form relatively strong N—H···Cl hydrogen bonds, see Table 3. This type of linkage justifies the reorientational motion of all the cations in the anionic voids as well as distortion of the IPA cations, resulting in a characteristic deviation of the central C atom from sp^3 hybridization, see Table 3. The disorder in the cationic substructure may indicate that hydrogen bonds do not act effectively at high temperatures. On the other hand, the interaction of amine groups with different $[Cd_3Cl_{10}]^{4-}$ ions may be the source of the cation disorder.

4.3. Phase II

In Phase II two independent Cd atoms are still located in two types of octahedral site, however, the site symmetry changes compared with Phase I. Cd1 occupies a general position while Cd2 lies at the center of symmetry. Thus, owing to the symmetry requirements in *Pbca*, the asymmetric unit should formally be written as a $[Cd_{1..5}Cl_5]^{2-}$ anion with two nonequivalent IPA cations. The environment of Cd1 is distorted, with one short contact to a terminal Cl1 atom of 2.4881 (8) Å and longer bonds to the remaining bridging atoms with an average bond length of 2.676 (6) Å. Cd2 has three distinct pairs of Cd2—Cl distances ranging from 2.5795 (6) to 2.6902 (6) Å, see Table 3.

An essential feature of this phase compared with the prototypic Phase I is a significant distortion of the polyanionic network that affects the shape of interstitial voids. While in Phase I the voids are rectangular in the *ac* plane with an angle of 90° between the Cl—Cl edges at the bridging vertex Cl atoms, in Phase II the angles deviate from the right angle value becoming 102.5 (1) and 79.1 (1)°. It is worth noting that such a pronounced change in the anionic network does not influence the cadmium coordination. The bond-valence sum for Cd1 does not change in the phase transition and is equal to 1.925, whereas the bond valences in both phases for the Cd2 position change slightly from 1.962 to 1.942.

The changes in anionic substructure affect the IPA cations. In Phase II all the IPA cations are still disordered. IPA-*A* from the parent Phase I is disordered over two IPA-*A* and IPA-*D* positions with 0.5 occupancy, whereas IPA-*B* is distributed over IPA-*B* and IPA-*C* with 0.45 (1) and 0.55 (1) occupancy. Fig. 5 presents the possible location of IPA cations in the structure in Phase II. All the H atoms from amine groups are involved in hydrogen bonding in this phase. The donor–acceptor distances range from 3.269 (6) to 3.586 (2) Å, whereas donor-to-acceptor angles range from 134 to 173°. In Phase II the disorder of the cations is still pronounced. Nevertheless, several hydrogen bonds are strong (Table 4).

The changes observed in the crystal structure of Phase II point to a displacive mechanism in the I–II phase transition. Nevertheless, the slight change in occupancy of IPA-*B* [s.o.f. = 0.45 (1)] and IPA-*C* [s.o.f. = 0.55 (1)] ions may also contribute to the mechanism. The relatively low entropy of this transformation [3 (1) J mol^{-1} K^{-1}] confirms its displacive char-

Table 3
Selected interatomic distances (Å), bond valence sums (S) and average Cd—Cl distances for $[(CH_3)_2CHNH_3]_4Cd_3Cl_{10}$ at 275, 320 and 375 K.

		375 K Phase I	320 K Phase II	275 K Phase III
Cd1	Cl1	2.4839 (5)	2.4881 (8)	2.5036 (14)
	Cl2	2.6372 (2)	2.6218 (6)	2.6175 (14)
	Cl9	2.6372 (2)	2.6435 (6)	2.6557 (15)
	Cl4	2.6824 (5)	2.6657 (7)	2.6703 (12)
	Cl3	2.7126 (3)	2.7094 (6)	2.6859 (15)
	Cl5	2.7126 (3)	2.7403 (6)	2.7155 (14)
S_{Cd1}		*1.925*	*1.925*	*1.928*
⟨Cd—Cl⟩		2.6443 (3)	2.6448 (3)	2.6414 (14)
Cd2	Cl4	2.5888 (4)	2.5795 (6)	2.5778 (11)
	Cl8	2.5888 (4)	2.5795 (6)	2.5813 (11)
	Cl5	2.6571 (3)	2.6245 (6)	2.6123 (18)
	Cl7	2.6571 (3)	2.6902 (6)	2.6130 (17)
	Cl3	2.6571 (3)	2.6902 (6)	2.6941 (17)
	Cl6	2.6571 (3)	2.6245 (6)	2.7116 (18)
S_{Cd2}		*1.942*	*1.962*	*1.962*
⟨Cd—Cl⟩		2.6343 (3)	2.6314 (6)	2.6331 (16)
Cd3	Cl10	2.4839 (5)	2.4881 (8)	2.4975 (14)
	Cl9	2.6372 (2)	2.6218 (6)	2.6121 (14)
	Cl2	2.6372 (2)	2.6435 (6)	2.6344 (14)
	Cl8	2.6824 (5)	2.6657 (7)	2.6613 (12)
	Cl6	2.7126 (3)	2.7403 (6)	2.7083 (15)
	Cl7	2.7126 (3)	2.7094 (6)	2.7529 (15)
S_{Cd3}		*1.925*	*1.925*	*1.904*
⟨Cd—Cl⟩		2.6443 (3)	2.6448 (6)	2.6444 (14)
		IPA-*A*	IPA-*A*	IPA-*A*1
		C1*A* C4*A* 1.499 (4)	C1*A* N1*AD* 1.504 (7)	C11*A* N1*A* 1.529 (2)
		C1*A* C3*A* 1.598 (5)	C1*A* C2*A* 1.43 (2)	C11*A* C21*A* 1.41 (2)
		C1*A* N2*A* 1.478 (3)	C1*A* C3*A* 1.42 (2)	C11*A* C31*A* 1.37 (2)
				IPA-*A*2
				C12*A* N1*A* 1.52 (2)
				C12*A* C22*A* 1.57 (2)
				C32*A* C12*A* 1.35 (2)
			IPA-*D*	IPA-*D*1
			C1*D* N1*AD* 1.405 (8)	N1*D* C11*D* 1.448 (2)
			C1*D* C3*D* 1.598 (11)	C11*D* C21*D* 1.35 (2)
			C1*D* C2*D* 1.634 (10)	C11*D* C31*D* 1.46 (2)
				IPA-*D*2
				N1*D* C12*D* 1.51 (2)
				C12*D* C32*D* 1.38 (2)
				C12*D* C22*D* 1.42 (2)
		IPA-*B*	IPA-*B*	IPA-*B*
		C1*B* C4*B* 1.319 (4)	C1*B* N1*B* 1.495 (9)	C1*B* N1*B* 1.446 (7)
		C1*B* C3*B* 1.409 (4)	C1*B* C2*B* 1.401 (11)	C1*B* C2*B* 1.387 (9)
		C1*B* N2*B* 1.435 (3)	C1*B* C3*B* 1.485 (10)	C1*B* C3*B* 1.431 (8)
			IPA-*C*	IPA-*C*
			C1*C* N1*C* 1.503 (6)	N1*C* C1*C* 1.501 (6)
			C1*C* C3*C* 1.545 (7)	C1*C* C2*C* 1.468 (8)
			C1*C* C2*C* 1.478 (7)	C1*C* C3*C* 1.491 (8)

acter, with some ordering contributing to the transformation entropy.

Symmetry-mode analysis has been performed for the anionic substructure using *AMPLIMODES* (Orobengoa *et al.*, 2009). It shows that the structure of Phase II has two distortion modes, a primary one that yields the space group *Pbca* and a secondary one that is compatible with the parent *Cmce* structure. The mode decomposition provided by *AMPLIMODES* shows the prevailing role of the primary distortion; from a total distortion amplitude[1] of 1.583 (1) Å the contribution of the primary component is 1.565 (2) Å. The primary distortion involves 8 of the 18 structural degrees of freedom present in the *Pbca* structure. The largest displacement in the distortion concerns the Cl2 atom and equals 0.437 (1) Å. Tables summarizing mode amplitudes are presented in the supplementary material.[2]

4.4. Phase III

Phase III adopts the orthorhombic space group $P2_12_12_1$ (No. 19). The asymmetric unit of the structure consists of three face-sharing $CdCl_6$ octahedra forming the $(Cd_3Cl_{10})^{4-}$ polyanion, which is counterbalanced by four symmetry-nonequivalent IPA ions. It is noteworthy that the configuration of the polyanionic network does not change much compared with Phase II. The geometry of the interstitial voids is preserved. After the phase transition, the angles between Cl—Cl edges at the bridging vertex Cl atoms change from 102.5 (1) to 103.6 (1)° and from 79.1 (1) to 78.3 (1)°. The transformation from Phase II to III is induced by the ordering of IPA cations. IPA-*A* and IPA-*D* are still disordered and adopt two noneqivalent positions in the crystal structure with 50% probability (IPA-*A*1, IPA-*A*2 and IPA-*D*1, IPA-*D*2). The conversion between positions 1 and 2 is different for the two cations. As IPA-*A* rotates along the C–N bond to switch from IPA-*A*1 to IPA-*A*2, IPA-*D* makes only a swinging motion. The bifurcated character of the N1*B*—H1*B*3···Cl interaction as well as the relatively large anisotropic displacement parameters also indicate the disorder of the IPA-*B* cation. It is, however, not as pronounced as in cations *A* and *D*. Only IPA-*C* is completely ordered; as a result it does not show deviations from sp^3 hybridization as do other cations (Fig. 5).

Ordering of IPA-*B* and IPA-*C* ions in Phase III indicates an order–disorder mechanism for the II–III transformation. In Phase III, however, the pronounced disorder of IPA-*A* and IPA-*D* cations still exists.

Symmetry-mode analysis of the II–III transition reveals that the deformation of the anionic substructure may also contribute to the mechanism of this transformation, although to a lesser extent than for the I–II transformation. The amplitude of the total distortion is lower compared with the I–II transition and equals 1.024 (1) Å; at the same time the number of structural degrees of freedom increases from 18 in Phase II to 39 in

[1] The total distortion amplitude is given by the square root of the sum of the square of all atomic displacements.
[2] Supplementary data for this paper are available from the IUCr electronic archives (Reference: KD5047). Services for accessing these data are described at the back of the journal.

Table 4
Hydrogen bonds in $[(CH_3)_2CHNH_3)]_4Cd_3Cl_{10}$ in phases I, II and III.

D—H$\cdots A$	$d(D$—H)	d(H$\cdots A$)	$d(D\cdots A)$	$\angle$ (DHA)
Phase I in *Cmce*, 375 K				
N2*B*—H2*B*2$\cdots$Cl3^{i}	0.89	2.68	3.336 (2)	132
N2*A*—H2*A*2$\cdots$Cl1	0.89	2.53	3.305 (2)	146
N2*A*—H2*A*3$\cdots$Cl3^{ii}	0.89	2.54	3.424 (2)	175
Phase II in *Pbca* 320 K				
N1*B*—H1*C*$\cdots$Cl2	0.88	2.58	3.269 (6)	134
N1*C*—H2*A*$\cdots$Cl4	0.89	2.76	3.502 (4)	141
N1*AD*—H1*D*$\cdots$Cl1	0.87	2.83	3.586 (2)	146
N1*AD*—H1*E*$\cdots$Cl3^{iii}	0.87	2.48	3.352 (2)	173
N1*AD*—H1*F*$\cdots$Cl1^{iv}	0.87	2.45	3.299 (3)	163
Phase III in $P2_12_12_1$ 275 K				
N1*A*—H1*A*1$\cdots$Cl7	0.89	2.61	3.496 (5)	177
N1*A*—H1*A*2$\cdots$Cl1^{v}	0.89	2.51	3.274 (4)	144
N1*A*—H1*A*2$\cdots$Cl2^{v}	0.89	2.88	3.418 (5)	121
N1*A*—H1*A*3$\cdots$Cl6^{vi}	0.89	2.82	3.376 (5)	122
N1*B*—H1*B*1$\cdots$Cl2^{vii}	0.89	2.46	3.319 (6)	161
N1*B*—H1*B*2$\cdots$Cl7^{viii}	0.89	2.77	3.411 (6)	130
N1*B*—H1*B*3$\cdots$Cl8	0.89	2.76	3.616 (8)	161
N1*B*—H1*B*3$\cdots$Cl6	0.89	2.77	3.303 (6)	120
N1*C*—H1*C*1$\cdots$Cl3	0.89	2.55	3.363 (5)	153
N1*C*—H1*C*2$\cdots$Cl6^{vi}	0.89	2.77	3.581 (6)	153
N1*C*—H1*C*3$\cdots$Cl4^{vi}	0.89	2.66	3.421 (7)	145
N1*C*—H1*C*3$\cdots$Cl9^{ix}	0.89	2.90	3.598 (5)	133
N1*D*—H1*D*1$\cdots$Cl3^{viii}	0.89	2.43	3.300 (5)	167
N1*D*—H1*D*2$\cdots$Cl10^{x}	0.89	2.44	3.290 (4)	160
N1*D*—H1*D*3$\cdots$Cl1	0.89	2.70	3.544 (7)	160

Symmetry codes: (i) $-x, y, z$; (ii) $x+\frac{1}{2}, y, -z+\frac{1}{2}$; (iii) $x+1, y, z$; (iv) $x+\frac{1}{2}, y, -z+\frac{1}{2}$; (v) $-x+\frac{5}{2}, -y, z-\frac{1}{2}$; (vi) $x+1, y, z$; (vii) $-x+\frac{3}{2}, -y, z-\frac{1}{2}$; (viii) $x-1, y, z$; (ix) $-x+\frac{5}{2}, -y, z+\frac{1}{2}$; (x) $-x+\frac{3}{2}, -y, z+\frac{1}{2}$.

Phase III. The maximum atomic displacement involves the Cl1 atom and equals 0.192 (1) Å. Two modes contribute to the distortion. The primary distortion of the $P2_12_12_1$ symmetry involving 21 degrees of freedom predominate over the secondary distortion of *Pbca* symmetry giving a distortion amplitude of 1.008 (3) Å *versus* 0.183 (3) Å.

The large entropy of the III–IV phase transition suggests further ordering of the cationic moieties with temperature lowering. The structure of Phase IV was not determined owing to crystal cracking and twinning accompanying the crystal system change from orthorhombic to monoclinic in the III–IV transformation.

5. Conclusions and summary

The substantial deformation of the anionic substructure that stands at the origin of the I–II phase transition and the significant contribution of atom displacements to the II–III transformation in $[(CH_3)_2CHNH_3]_4Cd_3Cl_{10}$ are rare examples of the displacive phase transition mechanism in chlorocadmate(II) systems. The inorganic part of the hybrid organic–inorganic material is generally a rigid framework that accommodates the soft organic substructure. Owing to their non-directional weak electrostatic and weak hydrogen interactions the organic counterions usually possess a significant degree of freedom and are thermally disordered in the crystal structure. Numerous phase transitions found in this class of material are more often induced by freezing of thermal motion and ordering of cations (Piecha *et al.*, 2007; Jakubas *et al.*, 2005, and references therein). In chlorocadmate(II) systems the order–disorder phenomena predominate over displacive mechanisms regardless of the dimensionality of the anionic substructure (Bonamartini-Corradi *et al.*, 1993; Jebari *et al.*, 1994; Battaglia *et al.*, 1992; Chapuis & Zuniga, 1980). In *N*-methylpropane-1,3-diammonium chlorocadmate, where the anionic substructure consists of infinite chains of $[(Cd_3Cl_{10})_n^{4n-}]_n$, the first-order phase transition at high temperature is induced by disordering of the hydrocarbon chains (Bonamartini-Corradi *et al.*, 1993). Propane-1,3-diammonium tetrachlorocadmate, with a two-dimensional perovskite-like substructure, reveals a first-order transformation which is also associated with disorder of the hydrocarbon chains (Battaglia *et al.*, 1992). The temperature-dependent disorder of the alkylammonium ions is responsible for the phase transitions in $[NH(CH_3)_3]CdCl_3$ (Chapuis & Zuniga, 1980).

Summarizing:

(i) A rare example of a two-dimensional cadmium(II) halide network with the formula $[(CH_3)_2CHNH_3]_4Cd_3Cl_{10}$ was synthesized.

(ii) The crystal undergoes three successive structural phase transitions at 353 (first order), 294 (second order) and 259 K (first order).

(iii) X-ray diffraction studies allowed us to find the structures of the phases and propose the molecular mechanism of successive transformations; the phase transition at 353 K is associated with the distortion of the anionic sublattice and has a displacive character, whereas the remaining transformations are dominated by order–disorder phenomena of the cationic substructure.

(iv) The entropy changes connected with particular phase transitions correspond well to the proposed mechanism of structure transformations.

References

Battaglia, L. P., Bonamartini-Corradi, A., Pelosi, G., Cramarossa, M. R., Manfredini, T., Pellacani, G. C., Motori, A., Saccani, A., Sandrolini, F. & Brigatti, M. F. (1992). *Chem. Mater.* **4**, 813–818.

Bonamartini-Corradi, A., Bruckner, S., Cramarossa, M. R., Manfredini, T., Menabue, L., Saladini, M., Sccani, A., Sandrolini, F. & Giusti, J. (1993). *J. Chem. Mater.* **5**, 90–97.

Brown, I. D. (1996). *J. Appl. Cryst.* **29**, 479–480.

Chaabane, I., Helf, F. & Guidara, K. (2008). *PMC Phys. B*, **1**, 11–18.

Chapuis, G. & Zuniga, F. J. (1980). *Acta Cryst.* B**36**, 807–812.

Costin-Hogan, Ch. E., Chen, E., Hughes, Ch.-L., Pickett, A., Valencia, R., Rath, N. P. & Beaty, A. (2008). *CrystEngComm*, **10**, 1910–1915.

Czapla, Z., Dacko, S., Krzewska, U. & Waśkowska, A. (1989). *Solid State Commun.* **71**, 139–141.

Czapla, Z., Przesławski, J. & Schlemmbach, H. (1994). *Solid State Commun.* **91**, 981–984.

Flack, H. D. (1983). *Acta Cryst.* A**39**, 876–881.

Ishihara, H., Krishnan, V. G., Dou, S., Paulus, H. & Weiss, A. (1994). *Z. Naturforsch. A Phys. Sci.* **49**, 213–222.

Jakubas, R., Piecha, A., Pietraszko, A. & Bator, G. (2005). *Phys. Rev. B*, **72**, 104107–104108.
Jebari, F., Becker, P. & Carabatos-Nédelec, C. (1994). *J. Raman Spectrosc.* **25**, 261–265.
Jian, F. F., Zha, P. S., Wang, Q. X. & Li, Y. (2006). *Inorg. Chim. Acta*, **359**, 1473–1477.
Krzewska, U., Jakubas, R., Dacko, S., Czapla, Z. & Waśkowska, A. (1992). *Acta Phys. Pol. A*, **81**, 379–384.
Lamhamdi, A., Mejdoubi, E., Fejfarová, K., Dušek, M. & El Bali, B. (2009). *Acta Cryst.* E**65**, m215–m216.
Marzili, L. G., Kistenmacher, T. J. & Eichhorn, G. L. (1980). *Metal Ions in Biology*, edited by T. G. Spiro, Vol. 1, p. 179. New York, Wiley.
Morosin, B. (1972). *Acta Cryst.* B**28**, 2303–2305.
Mulla-Osman, S., Michel, D., Voelkel, G. & Czapla, Z. (2000). *Phys. Status Solidi*, **219**, 9–13.
Noiret, I., Schamps, J., Real, F., Lamiot, J. & Hamzaoui, F. (2004). *Solid State Commun.* **131**, 543–548.
Orobengoa, D., Capillas, C., Aroyo, M. I. & Perez-Mato, J. M. (2009). *J. Appl. Cryst.* **42**, 820–833.
Oxford Diffraction (2005). *CrysAlis CCD*. Oxford Diffraction Ltd, Yarnton, Oxfordshire, England.
Oxford Diffraction (2008). *CrysAlis RED*, Version 1.170.132. Oxford Diffraction Ltd, Yarnton, Oxfordshire, England.
Peral, I., Madariaga, G., Pérez-Etxebarria, A. & Breczewski, T. (2000). *Acta Cryst.* B**56**, 215–225.
Piecha, A., Kinzhybalo, V., Jakubas, R., Baran, J. & Medycki, W. (2007). *Solid State Sci.* **9**, 1036–1048.
Sakida, S., Nakata, H. & Kawamoto, Y. (2003). *Solid State Commun.* **127**, 447–452.
Sheldrick, G. M. (2008). *Acta Cryst.* A**64**, 112–122.
Thorn, A., Willett, R. & Twamley, B. (2005). *Cryst. Growth Des.* **5**, 673–679.
Waśkowska, A., Lis, T., Krzewska, U. & Czapla, Z. (1990). *Acta Cryst.* C**46**, 1768–1770.